Research Article Vol. 5, No. 8 / August 2018 / Optica 910

Optical binding of two cooled micro-gyroscopes levitated in vacuum

Yoshihiko Arita,[1,2,6] Ewan M. Wright,[1,3] and Kishan Dholakia[1,3,4,5]

[1]SUPA, School of Physics & Astronomy, University of St Andrews, North Haugh, St Andrews KY16 9SS, UK
[2]Molecular Chirality Research Center, Chiba University, 1-33 Yayoi-cho, Inage-ku, Chiba-shi 263-0022, Japan
[3]College of Optical Sciences, The University of Arizona, Tucson, Arizona 85721-0094, USA
[4]Graduate School of Engineering, Chiba University, 1-33 Yayoi-cho, Inage-ku, Chiba-shi 263-0022, Japan
[5]e-mail: kd1@st-andrews.ac.uk
[6]e-mail: ya10@st-andrews.ac.uk

Received 29 January 2018; revised 4 June 2018; accepted 13 June 2018 (Doc. ID 320932); published 26 July 2018

Coupling between mesoscopic particles levitated in vacuum is a prerequisite for the realization of a large-scale array of particles in an underdamped environment as well as potential studies at the classical–quantum interface. Here, we demonstrate for the first time, to the best of our knowledge, optical binding between two rotating microparticles mediated by light scattering in vacuum. We investigate autocorrelations between the two normal modes of oscillation determined by the center-of-mass and the relative positions of the two-particle system. The inter-particle coupling, as a consequence of optical binding, removes the degeneracy of the normal mode frequencies, which is in good agreement with theory. We further demonstrate that the optically bound array of rotating microparticles retains their optical coupling during gyroscopic cooling, and exhibits cooperative motion whose center-of-mass is stabilized.

OCIS codes: (140.7010) Laser trapping; (350.4855) Optical tweezers or optical manipulation.
https://doi.org/10.1364/OPTICA.5.000910

1. INTRODUCTION

A central theme in levitated optomechanics is the trapping and control over all the degrees of freedom of mesoscopic particles levitated in vacuum. Such particles offer unprecedented opportunities for studies at the classical–quantum interface, enabled by the absence of direct dissipation and any physical contact. One of the primary goals is to bring an optically levitated particle to the quantum ground state by cooling its center-of-mass (CoM) motion via the light momentum transfer from the incident light field to the trapped particle [1–3]. Though yet to be attained, recent advances have shown a number of cooling mechanisms at play, and sub/millikelvin temperatures have been reached [4,5]. Importantly, such nano- and micromechanical oscillators exhibit high quality (Q)-factors, offering a force sensitivity of 20 zN $\mathrm{Hz}^{-1/2}$, which is sufficient to sense ultra-weak interactions, such as non-Newtonian gravitational forces [6,7].

While the majority of studies have focused on linear optical momentum transfer through radiation pressure, we have previously shown the transfer of spin angular momentum (SAM) to a trapped birefringent microparticle, "vaterite" in vacuum recording rotation rates of up to 10 MHz [8]. By including the rotational degrees of freedom, we have observed the effective cooling of microparticles through the gyroscopic effect in the absence of any "active" feedback method [8], in contrast to other recent studies [4,5]. Furthermore, a nanomechanical rotor with remarkably high-Q has been demonstrated by optically levitating a silicon nanorod and periodically driving its rotation with circularly polarized (CP) light [9]. The nanorod's motion is frequency locked to the periodic drive, resulting in ultra-stable rotations, with a stability close to that of the drive [10].

For a number of key studies, such as multiparticle entanglement and vacuum friction [11,12], the ability to individually trap, move, and rotate multiple particles at close proximity from one another in vacuum is essential with complete freedom over the transfer of both linear and SAM to each individual particle and ability to vary the inter-particle spacing. Recently, we have demonstrated the appropriate geometry for such a system using a spatial light modulator (SLM) [13]. By trapping and rotating two vaterite microparticles, we observed intensity modulation of the scattered light at the sum and difference frequencies with respect to the individual rotation rates. However, the key step is to conclusively demonstrate that the two particles interact and that their dynamical motion is inherently linked through a process known as optical binding [14–17]. This is what we present here with clear evidence of the optical coupling (binding) of two such trapped particles in vacuum, each acting as a harmonic oscillator. In our particular study, we make use of two rotating vaterite microparticles placed in close proximity to one another.

The reason to explore the optical binding of rotating anisotropic vaterite particles is twofold: first, if the particles are non-rotating, the resulting light scattering, which generally contains isotropic and anisotropic contributions, and associated optical binding will be anisotropic and depend on the relative orientation of the axes of the two birefringent particles (see Supplement 1, note S1 and Fig. S1, and Visualization 1). In contrast, for rotating particles, the anisotropic contribution of the scattered light can vanish upon temporal averaging, so that the particles act effectively as isotropic particles from the perspective of optical binding (see Supplement 1, note S1 and Fig. S2, and Visualization 2). Treating the rotating particles as effectively isotropic is valid as long as the rotation frequency far exceeds the frequencies associated with the effective optical binding. Second, a rotating body offers inertial stiffness, so the particles act as micro-gyroscopes, which prevents the particle instabilities that have been typically observed in optical traps operating at low pressures [7,18]. This allows us to operate in vacuum without a need for active feedback schemes.

Although considerable effort has been made in developing optically coupled oscillators [19,20], such studies to date are based on a clamped resonator, which imposes limits to thermalization and routes for decoherence. In this paper, we demonstrate optical binding between two rotating vaterite microparticles at close proximity and levitated in vacuum. The aerodynamic cross-coupling is greatly diminished when the mean-free-path (λ_{mfp}) of the surrounding gas molecules becomes larger than the particle size and approaches the inter-particle separation. At this gas pressure, the cross-coupling is entirely mediated by light scattering. We investigate autocorrelations between the two normal modes of oscillation, which are determined by the CoM and the relative positions of the two-particle system. Our theoretical model predicts that the coupling removes the degeneracy of the normal mode frequencies, which are measured by experiment and determine the cross-force coefficient. Furthermore, the optically bound array of rotating microparticles exhibits cooperative motion whose CoM is stabilized by gyroscopic cooling. Such an optically coupled and cooled array of micro-gyroscopes in levitated optomechanics may provide a future route for exploring multiparticle entanglement and quantum friction.

2. METHODS

A. Sample Preparation

The synthesis of vaterite crystals and the protocol for microparticle levitation are described elsewhere [21,22]. Vaterite is a positive uniaxial birefringent material with a spherical morphology. The particles have a mean radius of 2.2 μm ± 0.02 μm (2σ) and a surface roughness of 27.6 nm (2σ).

B. Experimental Setup

We trap and rotate two vaterite microparticles with two CP beams (continuous wave 1070 nm) in air ($\sim 10^3$ mBar). A holographic optical tweezers based on an SLM allows individual intensity control and three-dimensional positioning of two traps. Independent polarization control of traps is also achieved by generating beams of orthogonal polarization states that are subsequently combined at a polarizing beam displacer (PBD, Thorlabs, BD27) [13]. Crucially, the magnitude of the trapping forces in the lateral direction (xy plane) is much larger than the optical binding forces to assure the particles do not escape from their traps. The trap stiffness κ, however, is small enough to analyze the optical binding strength ξ. In order to meet these criteria, the optical power is maintained at a low level 25 mW, which is measured at the back aperture of the microscope objective (transmission 58% at 1070 nm) and is equally shared between the two trap sites, throughout the measurements. The chamber pressure is gradually reduced from atmospheric pressure to 10^{-2} mBar, so that both particles are rotating at rates ($\geq$ 20 kHz), greater than their trap frequencies ($\sim$0.66 kHz).

C. Detection Scheme

In order to simultaneously record the CoM positions of two particles, we use a fast CMOS camera (Mikrotron, EoSens MC1362) with a frame rate of 3493 fps synchronized with nanosecond laser pulses of 532 nm. This allows obtaining stroboscopic images of the two fast-rotating particles over a period of 1 s with a bandwidth of 1747 kHz, which is greater than the trap frequency typically $\sim$0.66 kHz (see Visualization 3 rendered at 25 frames/s (fps) from 3493 fps). CoM positions of each particle are subsequently analyzed at each frame to determine the two normal modes of oscillation. While the CMOS camera captures the translational motion, fast photodiodes (Thorlabs Inc., DET10C, InGaAs) are used to record the forward scattered light intensity from the two particles with a bandwidth >500 kHz. This allows tracking their rotational and translational motion simultaneously when reducing the chamber pressure. Due to the rotational Doppler effect, we observe modulation frequencies at twice the rotation rates, $2f_{\mathrm{r1}}$ and $2f_{\mathrm{r2}}$, of each particle [8]. In practice, f_{r1} and f_{r2} are also detected because of the variation in the photodiode signal induced by a small optical asymmetry on any given particle.

3. THEORY

In order to model the correlated motion between two optically bound microparticles, we employ the theoretical approach of Meiners and Quake [23] and Bartlett *et al.* [24], which includes the hydro-/aero-dynamic coupling between the particles, and we extend the theory to include the optical coupling between the particles in the underdamped case [25]. The optical binding scheme is shown in Fig. 1, where the two identical spheres (with mass of m and radius of a) are levitated by a pair of trapping beams propagating along the z axis. Transverse optical binding (along the x axis) perpendicular to the trapping beams is assumed to arise from the light scattering by the two particles, which causes the radiation pressure from one particle to the other and modifies each trapping potential. The spheres of radius a are taken to have an equilibrium particle separation R, and we label the deviations of the sphere centers from their equilibrium positions along the x axis by $x_j(t)$ where $j = 1, 2$ refers to each of the particles.

As alluded to in the introduction, we assume that the microparticles are rotating sufficiently rapidly that they may be treated as isotropic from the perspective of optical binding. Then further assuming that the micro-gyroscopes are tightly bound in the plane perpendicular to the beam propagation axis due to the light scattering, we hereafter concentrate on the longitudinal motions along the x axis. Adopting the notation of Bartlett *et al.* [24], the Langevin equations of motion for small amplitude sphere displacements including the inertial terms for the underdamped case can be written in matrix form as

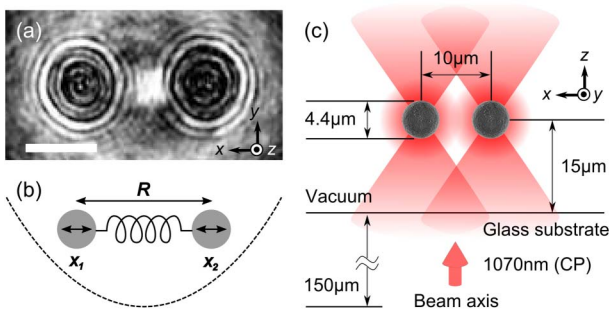

Fig. 1. Schematic showing the two normal modes of the bound array. (a) Stroboscopic image of two vaterite microparticles optically levitated and rotated in vacuum. The scale bar shows 5 μm. (b) The two normal modes of the bound array are depicted in the graphic, where R is the equilibrium particle separation of the particle centers, and $x_{1,2}$ indicate small displacements from the equilibrium position of the two particles along the x axis. The dashed line represents the potential related to the CoM motion of the two-particle system. The spring between the two spheres indicates the optical cross-interaction between the particles, the relative motion of them within the system. (c) The array is formed by the two foci of the trapping laser beams of 1070 nm propagating along the z axis within a range of the inter-particle separation (8 μm $\leq R \leq$ 11 μm).

$$mA_{11}\frac{d^2}{dt^2}\begin{pmatrix}x_1\\x_2\end{pmatrix}+\frac{d}{dt}\begin{pmatrix}x_1\\x_2\end{pmatrix}=\begin{pmatrix}A_{11}&A_{12}\\A_{12}&A_{11}\end{pmatrix}\begin{pmatrix}f_1(t)-\kappa x_1+\xi x_2\\f_2(t)-\kappa x_2+\xi x_1\end{pmatrix}, \quad (1)$$

where $A_{11}=1/(6\pi\mu a)$ and $A_{12}=1/(4\pi\mu R)$ are the longitudinal mobility factors with μ the residual gas viscosity. Here, $f_j(t)$ are noise sources with correlation functions

$$\langle f_j(t)\rangle = 0, \quad (2)$$

$$\langle f_i(\tau_1)f_j(\tau_2)\rangle = 2\delta_{ij}\lambda_j k_B T\delta(\tau_1-\tau_2), \quad (3)$$

which represent the fluctuating forces acting on the microparticles due to Brownian and other noise sources, e.g., beam pointing fluctuations, at effective temperature T.

The force terms proportional to the spring constant $\kappa \geq 0$ represent the direct force on a chosen sphere when that sphere is displaced while the other sphere is held fixed, and the force terms proportional to ξ describe the cross-force that arises on the chosen sphere at its equilibrium position when the other sphere is displaced. The force acting on a given sphere, e.g., sphere 1, is composed of two components along the x axis: a gradient force directed towards the beam focus, and a cross-force arising from the scattered light field caused by sphere 2 (see Fig. 1). Thus, the cross-force coefficient ξ is positive when longitudinal optical binding arises from the inter-particle scattering of the two spheres at close proximity. Balancing of these two forces (gradient and coupling) results in the equilibrium separation for the two optically binding spheres. If sphere 2 is displaced from its equilibrium position, the scattered light field amplitude produced by sphere 2 will be modulated. Consequently, sphere 1 will move its position to equilibrate the gradient and scattering forces along the x axis. The cross-force thus tends to correlate the motions of the two spheres.

To proceed, we introduce the normal mode coordinates for the CoM and the relative motion as $X_1=(1/\sqrt{2})(x_1+x_2)$ and $X_2=(1/\sqrt{2})(x_1-x_2)$. Based on the Langevin equations of motion for small amplitude sphere displacements, including the inertial terms for the underdamped case, we obtain the common harmonic oscillator form

$$\frac{d^2X_j}{dt^2}+\Gamma\frac{dX_j}{dt}+\omega_j^2X_j=\left(\frac{\mathcal{F}_j}{mA_{11}}\right), \qquad j=1,2, \quad (4)$$

where the damping coefficient $\Gamma=1/mA_{11}$, and the oscillator frequencies

$$\omega_1^2=\omega_0^2\left[1-\left(\frac{\xi}{\kappa}\right)\right](1+\epsilon), \quad (5)$$

$$\omega_2^2=\omega_0^2\left[1+\left(\frac{\xi}{\kappa}\right)\right](1-\epsilon), \quad (6)$$

with $\omega_0^2=\kappa/m$, and $\epsilon=A_{12}/A_{11}=3a/(2R)$. The theory developed here should be valid if the microparticle rotation rates are much larger than these oscillation frequencies $\omega_{1,2}$. These equations indicate that in the underdamped case, the two normal modes will experience the same damping but have different oscillation frequencies. In the extreme underdamped regime $\Omega_j \gg \Gamma/2$, we can approximate $\Omega_j=\omega_j$, which leads to the correlation functions

$$\langle X_j(t_1)X_j(t_2)\rangle=\frac{\lambda_j k_B T}{m^2A_{11}^2\Omega_j^2\Gamma}\cos(\Omega_j|t_1-t_2|)e^{-\Gamma|t_1-t_2|}, \quad (7)$$

where the frequencies Ω_j and the damping rate Γ may be determined from the experiment. Dividing Eqs. (5) and (6), and using $\Omega_j=\omega_j$ applicable to the low pressures of the experiment, and rearranging, we obtain

$$\frac{\xi}{\kappa}=\frac{[(1+\epsilon)/(1-\epsilon)-\Omega_1^2/\Omega_2^2]}{[(1+\epsilon)/(1-\epsilon)+\Omega_1^2/\Omega_2^2]}. \quad (8)$$

Thus, determining the normal mode frequencies from the experiment allows us to calculate the ratio (ξ/κ), and hence the cross-force coefficient ξ if κ is measured for a single trapped particle.

4. RESULTS AND DISCUSSION

In practice, when two particles are trapped and rotating in vacuum at the same optical power, the rotation rate of each particle can be different, depending on the particle size and mass, which alters the axial position of the particle along the beam axis. This variant modulates the optical torque as well as the Stokes drag torque acting on each particle, which yields different rotation rates typically within a factor of two. The beam separation R can be as small as 6.4 μm, which equates to a distance of 2 μm between the equators of the two particles, without loss of either of the particles from their trap sites at atmospheric pressure. This minimum distance, however, is dependent on the damping rate of the residual gas molecules. In order to avoid a loss of particles in vacuum, the beam separation is controlled within a range of 8 μm $\leq R \leq$ 11 μm. See Section 2 (Methods) for details. Visualization 3 [rendered at 25 fps from a measured frame rate at 3493 fps] shows two trapped vaterite microparticles ($a=2.2$ μm) with $R=9.8$ μm at a vacuum pressure of 0.081 mBar. These particles are co-rotating at a rate $\geq$ 20 kHz.

A. Cross-Force Constant

Figure 2(a) shows the two normal modes of $X_1 = (1/\sqrt{2})(x_1 + x_2)$ and $X_2 = (1/\sqrt{2})(x_1 - x_2)$ for the CoM (green) and the relative motion (red) of the two particles trapped with an inter-particle separation $R = 9.8$ μm at a chamber pressure $P = 0.081$ mBar, at which pressure $\lambda_{\mathrm{mfp}} = 0.428$ mm of the residual gas molecules is more than two orders of magnitude greater than the particle radius a and the separation R. At this gas pressure, aerodynamic coupling between the two particles is progressively diminished, and optical coupling is the primary cause of binding. Autocorrelation functions of each normal mode are compared in Fig. 2(b), where they decay at nearly the same rate but exhibit different oscillation frequencies [Figs. 2(c) and 2(d)]. The power spectra of each autocorrelation function X_1 and X_2 indicate their normal mode frequencies of $F_1 = 729.2$ Hz and $F_2 = 791.2$ Hz, respectively. It is rather straightforward to obtain ξ/κ by substituting these frequencies in Eq. (8), where $\Omega_j = 2\pi F_j$ $(j = 1, 2)$, which yields $\xi/\kappa = 0.40$. This means that the binding force constant is 40% of the trap stiffness of each particle.

B. Trap Stiffness

Based on the equipartition theorem, the trap stiffness of each particle is obtained by $\kappa = k_B T/\langle\sigma^2\rangle$, where k_B is the Boltzmann constant, T the temperature, and $\langle\sigma^2\rangle$ the mean square displacement or σ the standard deviation of the particle position distribution. Supplement 1, Fig. S3(a) shows the CoM position fluctuations of x_1 (green) and x_2 (red) from their equilibrium positions, where we obtain $\sigma_1 = 34.4$ nm and $\sigma_2 = 42.4$ nm for each particle (see also Supplement 1, note S2). Previously, we have determined the absorption coefficient of vaterite, which is 1.59×10^{-5} for a particle with a radius of 0.42 μm, which leads to the temperature rise of $4.2°\mathrm{CW}^{-1}$ [22]. It is reasonable to assume that $T = 296$ K kept at room temperature, given the optical power of ~7 mW at each trap site. Substituting σ and T, we obtain $\kappa_1 = 3.51$ pNμm^{-1} and $\kappa_2 = 2.30$ pNμm^{-1}, respectively. As $\xi/\kappa = 0.40$ in this experimental system, the binding force coefficient for each particle is $\xi_1 = 1.4$ pNμm^{-1}, and $\xi_2 = 0.92$ pNμm^{-1}.

C. Rotational Dynamics

By trapping and rotating two vaterite particles in close proximity in vacuum, we have observed inter-particle interactions, in the form of sum and difference frequency mixing, encoded onto the scattered light originating from the rotation of each particle [13]. As the particles rotate, their form asymmetries and optical anisotropies modulate, at the rotation frequency and its harmonics, the incident light field akin to a macroscopic Raman effect. Multiple scattering between the two particles further delivers a heterodyne signal, which displays the variety of parametric resonances that are observed in the previous experiment [13].

Figure 3(a) shows the power spectral density (PSD) of the incident light field scattered by two rotating microparticles with $R = 9.8$ μm at $P = 0.081$ mBar. We identify all the individual frequencies of rotational and translational motion of each particle with the aid of stroboscopic images acquired by the fast CMOS camera [see Subsection 2.C (Detection Scheme)]. It is evident that rotational frequencies $f_{rj} \geq 20$ kHz are more than 30 times larger than the translational frequencies $f_j \geq 0.66$ kHz. In such case, the anisotropic light scattering due to birefringence is time-averaged, and the particles are effectively isotropic from the viewpoint of optical binding (see Supplement 1, note S1 and Fig. S2). Figure 3(b) shows an expanded view of the power spectrum in the frequency range from 10 kHz–100 kHz showing the rotational

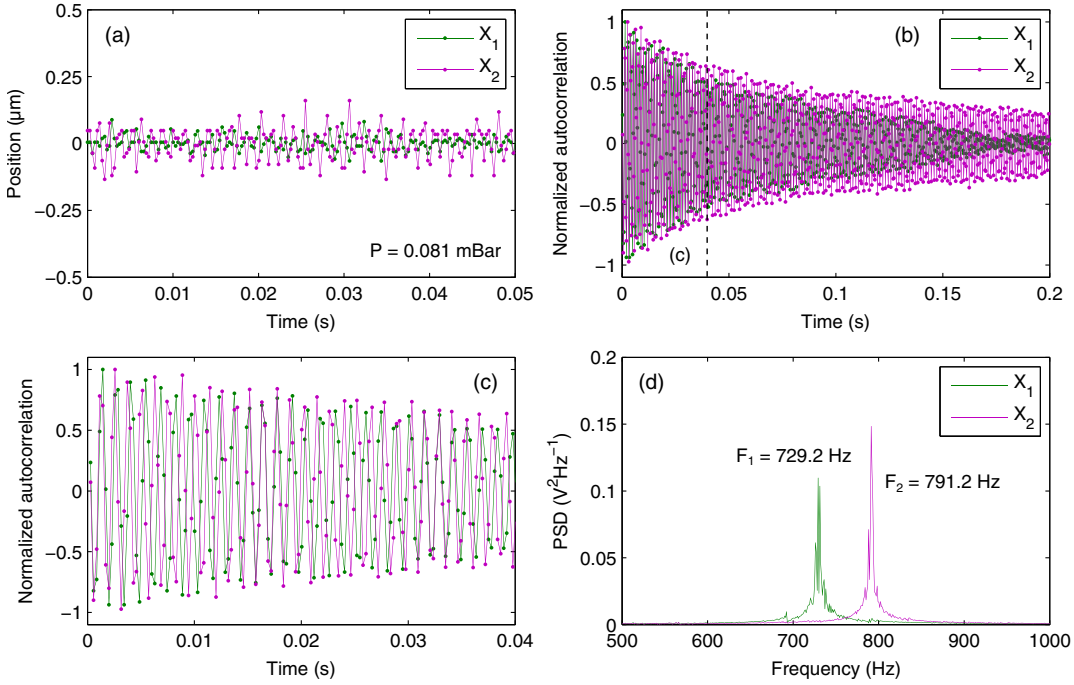

Fig. 2. Two normal modes of the bound array and each autocorrelation function. (a) Position fluctuations for the CoM normal mode $X_1 = (1/\sqrt{2})(x_1 + x_2)$, and the relative normal mode $X_2 = (1/\sqrt{2})(x_1 - x_2)$. (b) Normalized autocorrelation functions for X_1 (green) and X_2 (red). (c) An expanded view of (b) in the range of 0 s $\leq t \leq$ 0.04 s. (d) Power spectral densities of X_1 and X_2 around their normal mode frequencies.

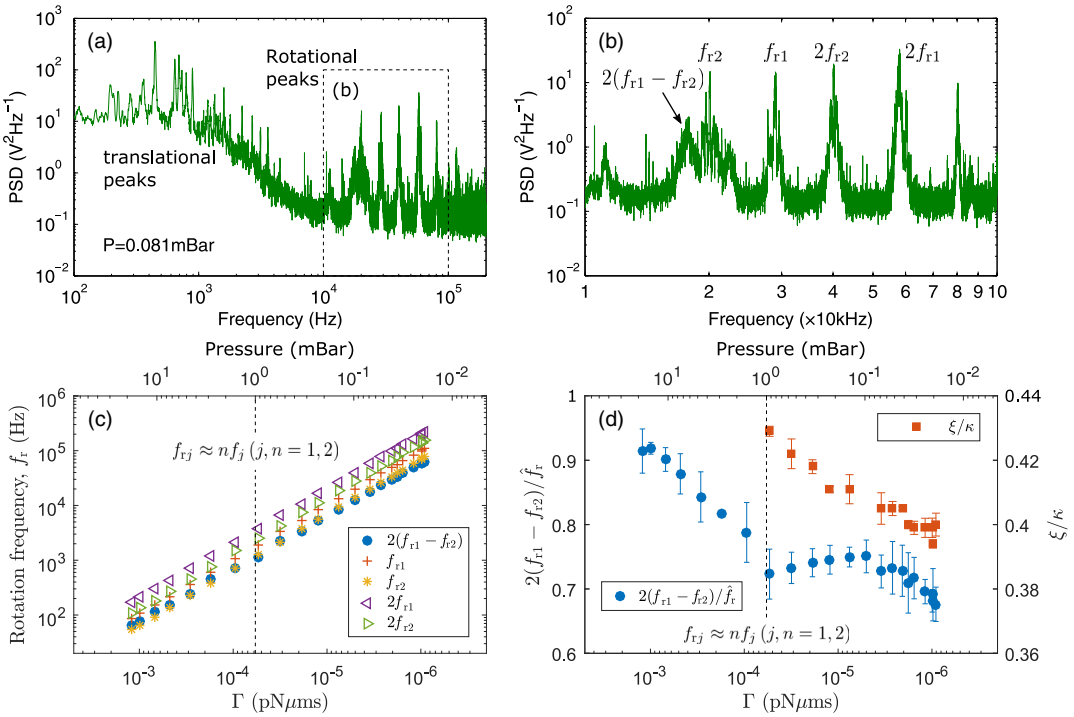

Fig. 3. Rotational and translational dynamics and ξ/κ of two rotating particles with $a = 2.2$ μm and with $R = 9.8$ μm at $P = 0.081$ mBar. (a) Power spectrum of the two rotating particles exhibiting their translational and rotational mode frequencies. (b) An expanded view in the frequency range of 10 kHz–100 kHz showing the two rotational frequencies of f_{r1}, f_{r2} and their second harmonics $2f_{r1}$, $2f_{r2}$ together with their DFG signal $2|f_{r1} - f_{r2}|$. (c) Rotational mode frequencies of the two particles for different damping coefficients Γ. (d) Normalized DFG signal $2|f_{r1} - f_{r2}|/\hat{f}_r$ and ξ/κ. The dashed lines in (c) and (d) mark the parametric resonances between the rotational and translational motion of the particles.

frequencies f_{r1}, f_{r2} of each particle and their second harmonics $2f_{r1}$, $2f_{r2}$ and the difference frequency generation (DFG) signal $2|f_{r1} - f_{r2}|$.

We further investigate a series of power spectra obtained from two rotating microparticles at different residual gas pressures in the range of 100 mBar–10^{-2} mBar, which is corresponding to the damping coefficients $\Gamma(P) = 8\pi\mu(P)r^3$. Here, $\mu(P)$ denotes the viscosity and is measured using a single vaterite particle with the same radius ($a = 2.2$ μm), rotating at a terminal rate $f_r(P)$. At this rotation rate, we have $\mu(P)f_r(P) = f_r(P_{air})\mu(P_{air})$ with $\mu(P_{air}) = 18.2 \times 10^{-6}$ Pas the viscosity of air. Figure 3(c) shows the rotational mode frequencies of the two particles, namely, f_{r1}, f_{r2}, $2f_{r1}$, and $2f_{r2}$, and the DFG signal $2|f_{r1} - f_{r2}|$, all of which are tracked at each power spectrum at different damping coefficients, and are increasing at the same rate as the chamber pressure is reduced.

D. Aerodynamic Coupling

The DFG is determined by the relative rotation rate of the two particles. If the particles are independent of each other and their rotation rates are dependent solely on the damping rate Γ of the surrounding gas molecules, the normalized DFG signal $2|f_{r1} - f_{r2}|/\hat{f}_r$, where $\hat{f}_r = (f_{r1} + f_{r2})/2$ is the mean rotation rate, must be constant over any Γ. The deviation from a constant value indicates inter-particle interactions such as binding [13]. Figure 3(d) shows the normalized DFG (blue circles) and the ratio of the cross-force coefficient ξ to the trap stiffness κ (orange circles) over a wide range of Γ. Interestingly, there appears a kink at a pressure around 1 mBar in the normalized DFG. This is due to mechanical couplings between the translational and rotational degrees of freedom of the trapped particles when the rotational frequency f_{rj} is resonant with the fundamental trap frequency f_j (a driven oscillator resonance) and with the second harmonic $2f_j$ (a parametric resonance), where $j = 1, 2$ denotes the individual particles [8]. In this regime, both traps are unstable (i.e., $T \gg 296$ K while $\kappa_{j=1,2}$ remains the same) due to these resonant excitations of the trapped particles. Beyond this transition, ξ/κ decreases from 0.43 to 0.40 with a decrease in Γ from 10^{-4} pNμms to 10^{-6} pNμms (over two orders of magnitude).

In Eq. (8), ξ/κ depends both on the aerodynamic coupling (ϵ) and the optical binding (Ω_1/Ω_2) terms. It is assumed in the theory that the two particles have the same mass m and hence the same value of $\Gamma = 1/A_{11}$, which results in a constant value of $\epsilon = 3a/(2R)$. However, this is not the case in general, as $m_1 \neq m_2$, which leads to slightly different damping rates $\Gamma_j = (m/m_j)/A_{11}$ in Eq. (8), where $j = 1, 2$, and the mass is redefined as $m = (m_1 + m_2)/2$, and would reflect the weak dependence of ξ/κ on Γ. In the underdamped case, however, it is possible that ϵ can be negligible, and Ω_1/Ω_2 determines the total binding force. Assuming κ remains constant over the Γ range examined, the fractional change in ξ/κ indicates a weak dependence of ξ on the aerodynamic coupling through residual gas molecules.

Although relatively minor compared to optical coupling, the rate of the aerodynamic coupling clearly depends on Γ. We further investigate the change in the relative position of the two trapped particles at different Γ to understand its mechanical effect (see Supplement 1, note S3 for details). Supplement 1, Figs. S4,

S5 indicate that the mean particle separation $R = 9.8$ μm changes within a range 9.65 μm $\leq R \leq$ 9.9 μm over pressures from sub-atmospheric 100 mBar to 10^{-2} mBar. Intriguingly, R exhibits its maximum at around 1 mBar, at which pressure both traps are in the parametric resonance regime. Beyond this pressure, the mean R decreases as the aerodynamic coupling or binding diminishes with the further decreasing Γ, where $\lambda_{\mathrm{mfp}} \gg a \approx R$.

E. ξ/κ and Particle Displacement

Optical binding can exhibit a long-range interaction force between microparticles [26]. It is intriguing to determine ξ/κ as a function of the inter-particle separation R. In this experiment, the chamber pressure is maintained at 0.037 mBar while changing the inter-particle separation in the range of 8.8 μm $\leq R \leq$ 10.8 μm by modulating the lateral position of one of the trapping beams using an SLM. Figure 4(a) shows ξ/κ (blue circles) and the particle displacement Δd (green triangles) at different particle separations R. By assuming that the trap stiffness κ remains constant for small displacements Δd, the cross-force constant ξ decays with the particle separation R, which is the same behavior as observed for Δd. It is evident that the particle displacement Δd increases with the binding force constant ξ. Here we note that ξ akin to κ is not the force per se but the spring constant for the cross-force for small displacements Δd from a stable equilibrium inter-particle separation R_e and is always a positive quantity with units of pNμm^{-1}. ξ/κ does not oscillate with R as the equilibrium separation R_e is changed. In contrast, the restoring force is measured for small displacements Δd only from a certain equilibrium inter-particle separation R_e where the force is zero. In this case, the restoring force oscillates with Δd due to the lateral optical binding force [27].

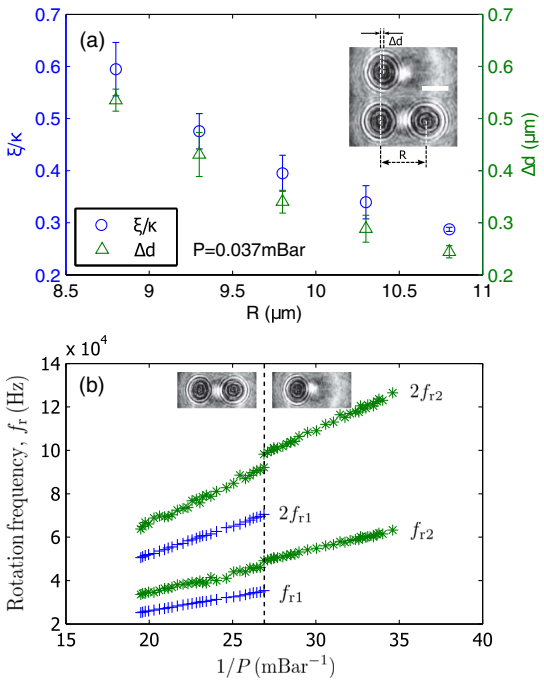

Fig. 4. Particle displacement and rotational frequency shift induced by optical binding. (a) ξ/κ and particle displacement Δd as a function of R at $P = 0.037$ mBar. Inset images show the particle displacement Δd induced by the presence of the other particle with $R = 9.8$ μm. (b) Rotational frequencies of the two rotating particles at different residual gas pressures. The frequency shift is induced at $1/P = 26.9$ mBar^{-1} (dashed line) by removing one of the particles. Inset images indicate the regimes of two-particle and single-particle systems.

The particle displacement induced by optical binding can alter the optical torque on the rotating particles. Figure 4(b) shows the rotation frequencies of $(f_{r1}, 2f_{r1})$ and $(f_{r2}, 2f_{r2})$ of each particle, depending on the residual gas pressure. These rotational mode frequencies scale inversely with the gas pressure P [8,28]. When one of the rotating particles leaves the trap at $P = 0.037$ mBar, the rotation rate of the remaining particle has increased by 2.73 kHz (+5.9%) from $f_{r2} = 46.39 \pm 0.05$ kHz (2σ) to $f'_{r2} = 49.12 \pm 0.05$ kHz (2σ). This is due to the fact that the remaining particle has restored its original position at the center of one of the trapping beams, where the field strength is larger than that at the position of the particle by the presence of the other particle. It is evident that the rotational and translational degrees of freedom of the trapped particles are coupled to the modified light field due to optical binding.

F. Gyroscopic Cooling and Optical Binding

Previously, we have demonstrated that rotational degrees of freedom of a levitated microparticle can offer a unique potential for cooling itself without any active feedback scheme [8], in contrast to previous experiments [4,5]. Akin to the motion of a spinning top, a rotating body offers inertial stiffness, which prevents the body from drifting from its desired orientation. As a result, this rotating sphere acts like a micro-gyroscope, stabilizing itself around the axis of rotation, in effect cooling the sphere to 40 K with respect to its CoM, where the CoM temperature T is deduced from the particle's Brownian dynamics.

We now progress to investigate if two rotating and optically bound particles may be cooled co-operatively as a two-particle system and still retain their optical coupling. We study the integral of the PSD $S(f)$ of the forward scattered light from the two trapped and rotating particles, which is measured by the fast photodiodes [see Subsection 2.C (Detection Scheme)]. This quantity is proportional to the mean square displacement of the particle $\langle\sigma^2\rangle$ and depends only upon trap stiffness κ and temperature T [8]:

$$\int_{-\infty}^{\infty} S(f)\mathrm{d}f = \langle\sigma^2\rangle = \frac{k_B T}{\kappa}. \tag{9}$$

This is a well-established means of determining κ and T [8]. Crucially, the trap stiffness κ linearly scales with optical power P, which is maintained at 25 mW (shared by the two traps) throughout this experiment while reducing the residual gas pressure from atmospheric pressure 10^3 mBar to 10^{-2} mBar. The CoM motion T of the two-particle system is calibrated by associating with the integral of the PSD measured at normal temperature (296 K) and pressure (10^3 mBar) or at NTP.

Figure 5(a) shows a series of power spectra of the incident light field scattered by two rotating particles (with an inter-particle separation $R = 9.8$ μm) measured at different residual gas pressures, each of which presents different rotation rates and PSDs. We monitor the CoM motion T of the two-particle system by integrating the PSD as a function of the mean rotation rate of the two particles [see Fig. 5(b)]. Due to parametric resonances, the two-rotating-particle system is heated up to 480 K (or becomes unstable) at around a pressure of 1 mBar [8]. Importantly, rotation stabilizes the traps and maintains the particles within their traps through this resonant transition. Beyond these resonances,

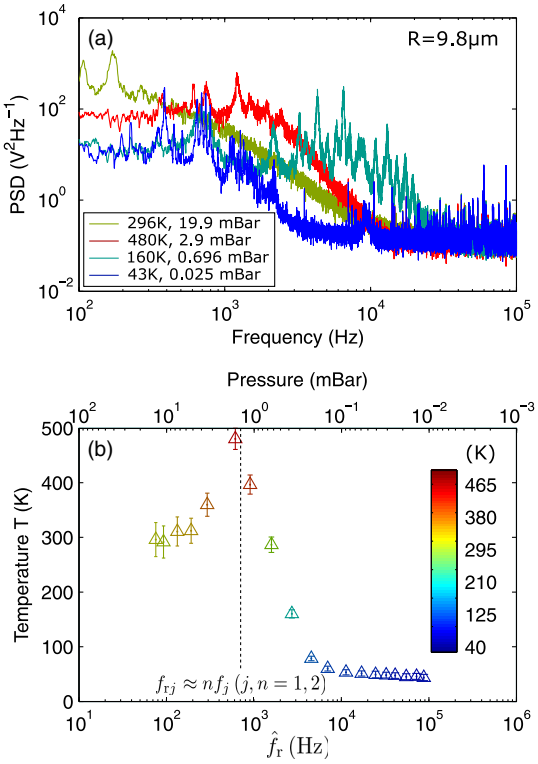

Fig. 5. Rotation-induced cooling of the two-particle system. (a) A series of power spectra of the two rotating microparticles showing different CoM motion temperature T. Each line color corresponds to a different T as indicated in (b), where T is calibrated at NTP. (b) CoM motion T as a function of the mean rotation rate $\hat{f}_r$ and the corresponding residual gas pressure P. The dashed line marks the parametric resonances.

T is seen to decrease, reaching a minimum value of 43 K at a mean rotation rate of $\hat{f}_r = 87$ kHz corresponding to a background pressure of 10^{-2} mBar. This is a similar cooling rate for a single rotating particle [8].

One can understand the cooling of the two-rotating-particle system as the composition of the two individual rotating particles, which are individually cooled due to the gyroscopic effect. However, these two particles are no longer individual, as they are optically bound and exhibit cooperative motion. This represents the first demonstration of a multi-particle system whose CoM motion is cooled via the gyroscopic effect. We note that it is possible to perform the experiment at a lower pressure down to 10^{-3} mBar with the current system [13], where optical binding and gyroscopic cooling will be maintained. Beyond that pressure, however, thermal nonlinearities may lead to particle instability, or heating may lead to particle loss [7]. This may limit the gyroscopic cooling ($T \geq 40$ K) and may require a feedback scheme for further cooling [4,29]. A more detailed future study will explore the interplay between binding and cooling of two or more microparticles to see the exact influence of each particle upon the other.

G. Electrostatic Forces

Finally, we briefly discuss electrostatic forces between charged microparticles compared to optical binding forces. Dielectric microparticles levitated in air/vacuum typically carry one to three elementary charges [30]. Here, we assume that the same number of N electrons Ne are evenly distributed on the surface of each vaterite microparticle ($a = 2.2$ μm) with an inter-particle separation $R = 9.8$ μm. In an exaggerated case with $N = 10$, the Coulomb force between two microparticles is 0.23 fN. We have measured the mean binding force constant $\hat{\xi} = 1.16$ pNμm^{-1} ± 0.05 pNμm^{-1} (2σ) [see Subsection 4.B (Trap Stiffness)] and the particle displacement $\Delta d = 0.33$ μm ± 0.03 μm (2σ) [see Fig. 4(a)] for $R = 9.8$ μm, which yields 0.38 pN± 0.05 pN (2σ). This optical binding force is more than three orders of magnitude larger than the Coulomb force (0.23 fN) between particles, carrying 10 charges each. Thus, the electrostatic forces are negligible in the present regime.

5. CONCLUSIONS

Optical binding of mesoscopic particles levitated in vacuum can pave the way towards the realization of a large-scale quantum bound array in cavity-optomechanics. Here we have demonstrated for the first time, to the best of our knowledge, an optically bound array of two micro-gyroscopes mediated by light scattering in vacuum. We have investigated autocorrelations between the two normal modes of oscillation, which are determined by the CoM and the relative positions of the two rotating microparticles. The inter-particle coupling removes the degeneracy of the normal mode frequencies, which is underpinned by theory. Furthermore, the optically bound array of two rotating microparticles exhibits cooperative motion whose CoM is stabilized by gyroscopic cooling.

We note that there are a number of experiments that our work can facilitate, which can be performed without the preparation of the particle in the quantum ground state. Quantum (or vacuum) friction is a prominent example of such a study [12]. Such an optically bound and cooled array of micro-gyroscopes may provide a platform for exploring multiparticle dynamics in underdamped systems close to the classical–quantum boundary.

Funding. Engineering and Physical Sciences Research Council (EPSRC) (EP/030017/1, EP/J01771X/1).

Acknowledgment. We thank Prof. Takashige Omatsu at Chiba University for useful discussions and Dr. Stephen Simpson and Professor Pavel Zemánek at ISI, Brno, Czech Republic for discussions on modeling of the experiment. The research data supporting this publication can be accessed at https://doi.org/10.17630/e6274faf-89b3-4d84-aa7d-30f68b7d5414.

See Supplement 1 for supporting content.

REFERENCES

1. P. F. Barker, "Doppler cooling a microsphere," Phys. Rev. Lett. **105**, 073002 (2010).
2. A. D. O'Connell, M. Hofheinz, M. Ansmann, R. C. Bialczak, M. Lenander, E. Lucero, M. Neeley, D. Sank, H. Wang, M. Weides, J. Wenner, J. M. Martinis, and A. N. Cleland, "Quantum ground state and single-phonon control of a mechanical resonator," Nature **464**, 697–703 (2010).
3. J. Chan, T. P. M. Alegre, A. H. Safavi-Naeini, J. T. Hill, A. Krause, S. Gröblacher, M. Aspelmeyer, and O. Painter, "Laser cooling of a nanomechanical oscillator into its quantum ground state," Nature **478**, 89–92 (2011).
4. T. C. Li, S. Kheifets, and M. G. Raizen, "Millikelvin cooling of an optically trapped microsphere in vacuum," Nat. Phys. **7**, 527–530 (2011).

5. J. Gieseler, B. Deutsch, R. Quidant, and L. Novotny, "Subkelvin parametric feedback cooling of a laser-trapped nanoparticle," Phys. Rev. Lett. **109**, 103603 (2012).
6. G. Ranjit, M. Cunningham, K. Casey, and A. A. Geraci, "Zeptonewton force sensing with nanospheres in an optical lattice," Phys. Rev. A **10593**, 053801 (2016).
7. J. Gieseler, L. Novotny, and R. Quidant, "Thermal nonlinearities in a nanomechanical oscillator," Nat. Phys. **9**, 806–810 (2013).
8. Y. Arita, M. Mazilu, and K. Dholakia, "Laser-induced rotation and cooling of a trapped microgyroscope in vacuum," Nat. Commun. **4**, 2374 (2013).
9. S. Kuhn, P. Asenbaum, A. Kosloff, M. Sclafani, B. A. Stickler, S. Nimmrichter, K. Hornberger, O. Cheshnovsky, F. Patolsky, and M. Arndt, "Cavity-assisted manipulation of freely rotating silicon nanorods in high vacuum," Nano Lett. **15**, 5604–5608 (2015).
10. S. Kuhn, A. Kosloff, B. A. Stickler, F. Patolsky, K. Hornberger, M. Arndt, and J. Millen, "Full rotational control of levitated silicon nanorods," Optica **4**, 356–360 (2017).
11. A. Manjavacas and F. J. G. de Abajo, "Vacuum friction in rotating particles," Phys. Rev. Lett. **105**, 113601 (2010).
12. R. K. Zhao, A. Manjavacas, F. J. G. de Abajo, and J. B. Pendry, "Rotational quantum friction," Phys. Rev. Lett. **109**, 123604 (2012).
13. Y. Arita, M. Mazilu, T. Vettenburg, E. M. Wright, and K. Dholakia, "Rotation of two trapped microparticles in vacuum: observation of optically mediated parametric resonances," Opt. Lett. **40**, 4751–4754 (2015).
14. K. Dholakia and P. Zemanek, "Colloquium: gripped by light: optical binding," Rev. Mod. Phys. **82**, 1767–1791 (2010).
15. M. Guillon and B. Stout, "Optical trapping and binding in air: imaging and spectroscopic analysis," Phys. Rev. A **77**, 023806 (2008).
16. S. Maayani, L. L. Martin, and T. Carmon, "Optical binding in white light," Opt. Lett. **40**, 1818–1821 (2015).
17. O. Brzobohatý, T. Čižmár, V. Karásek, M. Šiler, K. Dholakia, and P. Zemánek, "Experimental and theoretical determination of optical binding forces," Opt. Express **18**, 25389–25402 (2010).
18. J. Millen, T. Deesuwan, P. F. Barker, and J. Anders, "Nanoscale temperature measurements using non-equilibrium Brownian dynamics of a levitated nanosphere," Nat. Nanotechnol. **9**, 425–429 (2014).
19. Y. L. Li, J. Millen, and P. F. Barker, "Simultaneous cooling of coupled mechanical oscillators using whispering gallery mode resonances," Opt. Express **24**, 1392–1401 (2016).
20. R. Madugani, Y. Yang, J. M. Ward, V. H. Le, and S. Nic Chormaic, "Optomechanical transduction and characterization of a silica microsphere pendulum via evanescent light," Appl. Phys. Lett. **106**, 241101 (2015).
21. Y. Arita, A. W. McKinley, M. Mazilu, H. Rubinsztein-Dunlop, and K. Dholakia, "Picoliter rheology of gaseous media using a rotating optically trapped birefringent microparticle," Anal. Chem. **83**, 8855–8858 (2011).
22. Y. Arita, J. M. Richards, M. Mazilu, G. C. Spalding, S. E. S. Spesyvtseva, D. Craig, and K. Dholakia, "Rotational dynamics and heating of trapped nanovaterite particles," ACS Nano **10**, 11505–11510 (2016).
23. J. C. Meiners and S. R. Quake, "Direct measurement of hydrodynamic cross correlations between two particles in an external potential," Phys. Rev. Lett. **82**, 2211–2214 (1999).
24. P. Bartlett, S. I. Henderson, and S. J. Mitchell, "Measurement of the hydrodynamic forces between two polymer-coated spheres," Philos. Trans. R. Soc. London A **359**, 883–895 (2001).
25. N. K. Metzger, R. F. Marchington, M. Mazilu, R. L. Smith, K. Dholakia, and E. M. Wright, "Measurement of the restoring forces acting on two optically bound particles from normal mode correlations," Phys. Rev. Lett. **98**, 068102 (2007).
26. M. Mazilu, A. Rudhall, E. M. Wright, and K. Dholakia, "An interacting dipole model to explore broadband transverse optical binding," J. Phys. **24**, 464117 (2012).
27. M.-T. Wei, J. Ng, C. T. Chan, and H. D. Ou-Yang, "Lateral optical binding between two colloidal particles," Sci. Rep. **6**, 38883 (2016).
28. Y. Arita, M. Chen, E. M. Wright, and K. Dholakia, "Dynamics of a levitated microparticle in vacuum trapped by a perfect vortex beam: three-dimensional motion around a complex optical potential," J. Opt. Soc. Am. B **34**, C14–C19 (2017).
29. F. Monteiro, S. Ghosh, E. C. van Assendelft, and D. C. Moore, "Optical rotation of levitated spheres in high vacuum," Phys. Rev. A **97**, 051802 (2018).
30. J. Millen, P. Z. Fonseca, T. Mavrogordatos, T. S. Monteiro, and P. F. Barker, "Cavity cooling a single charged levitated nanosphere," Phys. Rev. Lett. **114**, 123602 (2015).